A&A 578, A119 (2015)
DOI: 10.1051/0004-6361/201526009

Astronomy & Astrophysics

A search for water maser emission toward obscured post-AGB star and planetary nebula candidates⋆

J. F. Gómez[1], J. R. Rizzo[2], O. Suárez[3], A. Palau[4], L. F. Miranda[1], M. A. Guerrero[1], G. Ramos-Larios[5], and J. M. Torrelles[6,7]

[1] Instituto de Astrofísica de Andalucía, CSIC, Glorieta de la Astronomía s/n, 18008 Granada, Spain
e-mail: jfg@iaa.es
[2] Centro de Astrobiología, INTA-CSIC, Carretera M-108, km. 4, 28850 Torrejón de Ardoz, Madrid, Spain
[3] UMR 6525 H.Fizeau, Université de Nice Sophia Antipolis, CNRS, OCA. Parc Valrose, 06108 Nice Cedex 2, France
[4] Centro de Radioastronomía y Astrofísica, UNAM, Campus Morelia, Apdo. Postal 3-72, Morelia, 58089 Michoacán, Mexico
[5] Instituto de Astronomía y Meteorología, CUCEI, Universidad de Guadalajara, Av. Vallarta No. 2602, Col. Arcos Vallarta, 44130 Guadalajara, Jalisco, Mexico
[6] Institut de Ciències de l'Espai (CSIC)/IEEC, 08034 Barcelona, Spain
[7] Institut de Ciències del Cosmos, Universitat de Barcelona (associated unit of CSIC through the ICE), Martí i Franquès 1, 08028 Barcelona, Spain

Received 3 March 2015 / Accepted 17 April 2015

ABSTRACT

Context. Water maser emission at 22 GHz is a useful probe for studying the transition between the nearly spherical mass loss in the asymptotic giant branch (AGB) to a collimated one in the post-AGB phase. In their turn, collimated jets in the post-AGB phase could determine the shape of planetary nebulae once photoionization starts.
Aims. We intend to find new cases of post-AGB stars and planetary nebulae (PNe) with water maser emission, including some especially interesting and rare types: water fountains (evolved objects with high velocity collimated jets traced by water masers) or water-maser-emitting PNe. Since previous studies have shown a higher detection rate of water maser emission in evolved objects that are optically obscured, we selected a sample that contains a significant fraction of post-AGB and young PN candidate sources showing signs of strong obscuration.
Methods. We searched for water maser emission in 133 evolved objects using the radio telescopes in Robledo de Chavela, Parkes, and Green Bank.
Results. We detected water maser emission in 15 sources of our sample, of which seven are reported here for the first time (IRAS 13483−5905, IRAS 14249−5310, IRAS 15408−5413, IRAS 17021−3109, IRAS 17348−2906, IRAS 17393−2727, and IRAS 18361−1203). We identified three water fountain candidates: IRAS 17291−2147, with a total velocity spread of ≃96 km s^{-1} in its water maser components and two sources (IRAS 17021−3109 and IRAS 17348−2906) that show water maser emission whose velocity lies outside the velocity range covered by OH masers. We have also identified IRAS 17393−2727 as a possible new water-maser-emitting PN.
Conclusions. The detection rate is higher in obscured objects (14%) than in those with optical counterparts (7%), which is consistent with previous results. Water maser emission seems to be common in objects that are bipolar in the near-IR (43% detection rate in such sources). The water maser spectra of water fountain candidates like IRAS 17291−2147 show significantly fewer maser components than others (e.g., IRAS 18113−2503). We speculate that most post-AGBs may show water maser emission with wide enough velocity spread (≥100 km s^{-1}) when observed with enough sensitivity and/or for long enough periods of time. Therefore, it may be necessary to single out a special group of "water fountains", probably defined by their high maser luminosities. We also suggest that the presence of both water and OH masers in a PN is a better tracer of its youth, than is the presence of just one of these species.

Key words. masers – surveys – stars: AGB and post-AGB – stars: mass-loss – planetary nebulae: general

1. Introduction

Maser emission is present in different astrophysical environments (e.g., star-forming regions, evolved stars, active galactic nuclei), and it is a signpost of energetic phenomena, since strong shocks or intense radiation fields are required to produce the population inversion of energy levels necessary for maser amplification. In the particular case of evolved stars, maser emission is common in the circumstellar structures of O-rich sources during the asymptotic giant branch (AGB) phase (Lewis 1989), characterized by strong mass loss.

Especially conspicuous is the presence of double-peaked OH maser profiles (see, e.g., Sevenster et al. 1997). It is widely accepted that maser emission in these sources traces the expanding circumstellar envelope (Reid et al. 1977). The velocity separation between the OH peaks is ∼30 km s^{-1}, and it provides a good estimate of the expansion velocity of the envelope (the expansion velocity should be half of the OH peak separation) at the location of the OH maser emission (≳10^3 AU, Reid & Moran 1981), whereas the mean OH velocity accurately traces the stellar velocity along the line of sight. SiO and H_2O masers are also widespread in AGB stars, and they seem to arise from gas volumes closer to the star than the OH emission. These inner zones may have higher expansion velocities, but they also

⋆ Table 1 and Fig. 1 are available in electronic form at http://www.aanda.org

show larger velocity gradients. Since maser emission requires a sufficient column density of molecules with coherent velocities along the line of sight, SiO and H_2O masers tend to arise from gas moving in directions closer to the plane of the sky than for emitting OH masers, and the observed velocity along the line of sight is lower. The result is that the velocity components in the spectra of SiO and H_2O masers are contained within the velocity range of OH.

Maser emission is also present in subsequent phases (Engels 2002), but with much lower prevalence. When the AGB mass loss stops and the star enters the post-AGB phase, the maser emission from the expanding envelope is expected to disappear on timescales of around 10, 100, and 1000 yr for SiO, H_2O, and OH masers, respectively (Lewis 1989; Gómez et al. 1990). However, although the mass-loss rates during the post-AGB phase are much lower ($\lesssim 10^{-7}$ $M_\odot$ yr^{-1}, Vassiliadis & Wood 1994; Blöcker 1995b) than during the AGB (up to $\simeq 10^{-4}$ $M_\odot$ yr^{-1}, Vassiliadis & Wood 1993; Blöcker 1995a), it may take the form of high-velocity, collimated jets, which also carry enough energy to pump maser emission. Therefore, this emission is an excellent tool for studying the transition from nearly spherical to collimated mass loss. This is a key issue, since the effect of jets on the circumstellar envelopes during the post-AGB phase may determine the shape of PNe once ionization starts.

The paradigmatic examples of collimated jets traced by maser emission are the small group of sources called "water fountains" (Imai 2007). These are objects (most of them post-AGB stars) whose H_2O maser emission traces high-velocity ($\gtrsim 100$ km s^{-1}), collimated jets, with very short dynamical ages ($\lesssim 100$ yr). These objects are usually identified by the large velocity spread in their water maser components (up to $\simeq 500$ km s^{-1} Gómez et al. 2011), amply surpassing the velocity range of OH emission. A firm confirmation of their nature as "water fountains" requires interferometric observations, to ascertain that there is no confusion of maser components from different sources within a single-dish beam and to determine the bipolar nature of the maser emission, as expected from a jet. The short dynamical ages of "water fountains" jets suggest that they may represent one of the first manifestations of collimated mass loss in evolved stars. Thirteen "water fountains" have been confirmed so far (Gómez et al. 2015b).

When the central star is hot enough to photoionize the surrounding envelope, the source enters the planetary nebula (PN) phase. The presence of maser emission is uncommon in PNe, and it may be restricted to the very first stages of this phase. No PN has been found to harbor SiO masers, while only six have been confirmed so far as OH-maser emitters (Uscanga et al. 2012), usually known as OHPNe (Zijlstra et al. 1989), and five have H_2O masers (H_2O-PNe, Miranda et al. 2001; de Gregorio-Monsalvo et al. 2004; Gómez et al. 2008; Uscanga et al. 2014; Gomez et al. 2015a). Of these, two harbor both OH and H_2O masers. Maser emission in PNe seems to be exclusively associated to bipolar objects (Uscanga et al. 2014), and it has been suggested that maser-emitting PNe may have "water fountains" as their precursors (Gómez et al. 2008). However, as opposed to "water fountains", OH and H_2O maser emission in PNe shows very low velocities (with the notable exception of IRAS 15103−5754, Gomez et al. 2015a), and may primarily trace circumstellar toroidal structures. In any case, masers in PNe may not be the remnant of those in the AGB phase, but seem to be related to mass-loss processes started in subsequent phases. This is because, on the one hand, the short timescale of survival of H_2O maser emission after the AGB (100 yr) would prevent its detection in PNe. On the other hand, while OH masers pumped in the AGB may still survive in extremely young PNe, some relatively evolved PNe are also OH emitters (Uscanga et al. 2012), indicating that new OH masers can appear after the end of the AGB.

In summary, maser emission is a good tracer of energetic mass-loss processes in objects on their way to becoming PNe. With this in mind, we undertook an extensive and sensitive search for water maser emission in post-AGB stars and young PNe (Suárez et al. 2007, 2009). From these past observations, it was evident that water maser emission appears to be more common in optically obscured sources. In this paper we present a new sensitive survey for water maser emission. A significant portion of the sample consists of post-AGB and young PN candidate sources showing signs of strong obscuration.

2. Source sample

The observed sources are listed in Table 1. They comprise most of the sources in Ramos-Larios et al. (2009). They are post-AGB stars and PN candidates with the IRAS color criteria of Suárez et al. (2006) and with signs of strong optical obscuration. We have also included some optically visible post-AGB stars from Suárez et al. (2006) that were not included in our previous water maser observations of Suárez et al. (2007, 2009) or for which those observations had poor sensitivity. There are previous water maser observations of some sources in our sample, which are also cited in Table 1 (including those by Yoon et al. 2014, who also selected 76 sources from Ramos-Larios et al. 2009 as part of their sample of 164 post-AGB candidates), although our data have significantly higher sensitivity (over one order of magnitude more in most cases). A total of 133 sources were observed.

3. Observations

We observed the 6_{16}−5_{23} transition of H_2O (rest frequency = 22 235.08 MHz) using three different telescopes: the DSS-63 antenna (70 m diameter) at the Madrid Deep Space Communications Complex (MDSCC) near Robledo de Chavela (Spain), the 64 m antenna at the Parkes Observatory of the Australia Telescope National Facility (ATNF), and the 100 m Robert C. Byrd Green Bank Telescope (GBT) of the National Radio Astronomy Observatory. The observed positions, rms noise per spectral channel, and observing dates are listed in Table 1. All spectra were centered at $V_{\rm LSR}$ = 0.0 km s^{-1}. The only exceptions are the spectra toward IRAS 18113−2503, which were formed from two independent integrations centered on different velocities, to cover the whole velocity range of detected components better. In the case of the Robledo data, for which Doppler tracking was not available, the central velocity could vary within $V_{\rm LSR} = 0.0 \pm 0.5$ km s^{-1}. All spectra were corrected for the elevation-dependent gain of each telescope and for atmospheric opacity.

3.1. Robledo de Chavela

The DSS-63 antenna at MDSCC has a diameter of 70 m, providing a half-power beam width of $\simeq 42''$ at this frequency. We used a 384-channel spectrometer covering a bandwidth of 16 MHz ($\simeq 216$ km s^{-1} with $\simeq 0.6$ km s^{-1} spectral resolution). Spectra were taken in position-switching mode, and only left-handed circular polarization was available. The total integration time was typically 30 min (on + off). Initial calibration, along with gain and opacity corrections, was carried out with procedures written in Interactive Data Language (IDL). Subsequent data reduction

Table 2. Water maser detections.

IRAS	V_{peak} [a] (km s^{-1})	V_{min} [b] (km s^{-1})	V_{max} [c] (km s^{-1})	S_{peak} [d] (Jy)	$\int S_\nu dv$ [e] (Jy km s^{-1})	Date
13483−5905	+24.0 ± 0.4	−27.0	+27.0	2.78 ± 0.17	21.3 ± 0.9	13-Sep-2008
14249−5310	−10.1 ± 0.4	−19.8	−9.7	0.42 ± 0.14	0.42 ± 0.20	13-Sep-2008
15408−5413	−82.6 ± 0.4	−85.1	−75.9	52.44 ± 0.17	59.0 ± 0.5	15-Sep-2008
15452−5459	−76.3 ± 0.4	−79.2	−35.4	1.62 ± 0.15	10.9 ± 0.8	12-Sep-2008
17021−3109	+13.5 ± 0.6	+13.2	+13.5	0.26 ± 0.04	0.20 ± 0.06	21-Mar-2010
17291−2147	−15.0 ± 0.6	−18.8	−13.9	0.59 ± 0.13	2.62 ± 0.17	06-Jun-2008
	−14.5 ± 0.3	−28.0	+69.5	3.381 ± 0.022	5.49 ± 0.07	21-Mar-2010
17348−2906	+1.0 ± 0.3	+0.7	+9.2	0.23 ± 0.04	0.52 ± 0.10	03-Mar-2010
17393−2727	−107.6 ± 0.3	−108.0	−106.7	1.07 ± 0.04	0.90 ± 0.04	03-Mar-2010
18039−1903	+153.1 ± 0.3	+150.8	+165.9	3.98 ± 0.03	5.38 ± 0.07	01-Mar-2010
18113−2503	−147.8 ± 0.3	−154.1	+334.5[f]	119.67 ± 0.03	845.9 ± 0.3	03-Mar-2010
	−147.6 ± 0.3	−154.2	+345.5	111.92 ± 0.04	812.8 ± 0.4	21-Mar-2010
18361−1203	+12.5 ± 0.3	+11.8	+13.5	0.101 ± 0.023	0.19 ± 0.04	01-Mar-2010
	+12.8 ± 0.3	+11.8	+13.5	0.14 ± 0.03	0.15 ± 0.04	21-Mar-2010
18596+0315	+61.6 ± 0.3	+59.6	+62.2	0.72 ± 0.03	0.69 ± 0.04	07-Mar-2010
19134+2131	−9.2 ± 0.3	−124.8	−7.9	3.60 ± 0.03	5.51 ± 0.17	07-Mar-2010
19190+1102	+59.3 ± 0.3	−55.3	+90.5	25.64 ± 0.03	164.94 ± 0.19	07-Mar-2010
19319+2214	+15.1 ± 0.6	+15.1	+15.1	0.35 ± 0.12	0.35 ± 0.14	28-Jun-2008
	+15.5 ± 0.3	+8.8	+33.6	0.547 ± 0.024	1.95 ± 0.08	07-Mar-2010

Notes. [a] LSR velocity of the peak emission in each spectrum. The uncertainty is the channel width. [b] Minimum LSR velocity of the detected emission. [c] Maximum LSR velocity of the detected emission. [d] Flux density of the peak emission, with 2σ uncertainty. [e] Velocity-integrated flux density of the spectrum, with 2σ uncertainty. [f] There is detected emission very close to the redshifted edge of the bandpass, so we probably missed some components beyond that edge.

was performed using the CLASS package, which is part of the GILDAS software.

3.2. Parkes

The 64 m antenna at the Parkes Observatory has a beamwidth of ≃1.3′ at this frequency. Both right and left circular polarization were observed simultaneously. As a backend, we used the Multibeam Correlator, covering a bandwidth of 64 MHz (i.e., velocity coverage ≃863 km s^{-1}) with 2048 spectral channels for each polarization, thus yielding a spectral resolution of 31.25 kHz (0.42 km s^{-1}). The observations were taken in position-switching mode with a total integration time (on+off) of 30 min. Data reduction was carried out with the libraries of the ATNF Spectral line Analysis Package (ASAP) included within the Common Astronomy Software Applications (CASA) package.

3.3. Green Bank

The 1.3 cm receiver of the GBT comprised four beams, arranged in two pairs that could be tuned independently. We used one such pair, with a separation of 178.8″ between the beams, to simultaneously observe an on- and off-source position in dual polarization. Antenna nodding between the two beams was used to subtract atmospheric and instrumental contributions. We selected two spectral windows, one centered on the water line and the other one comprising three methanol lines (whose results were presented in Gómez et al. 2014). The bandwidth of each spectral window was 50 MHz (≃674 km s^{-1} velocity coverage) sampled over 8192 channels (∼0.082 km s^{-1} velocity resolution). The half-power beam width of this 100 m telescope was 34″ at the frequency of the water line. The integration time per source was approximately four minutes, and all of it was effectively on-source time, because of the use of the antenna-nodding with dual beams. The data was reduced with the GBTidl package. Final spectra were smoothed up to a resolution of 0.33 km s^{-1}.

4. Results

We have detected water maser emission in 15 sources of our sample, of which seven are reported here for the first time (IRAS 13483−5905, IRAS 14249−5310, IRAS 15408−5413, IRAS 17021−3109, IRAS 17348−2906, IRAS 17393−2727, and IRAS 18361−1203). We also detected water maser emission in the spectrum taken toward IRAS 19071+0857 with both Robledo and GBT telescopes. However, follow-up observations with the Very Large Array (VLA) have shown that the maser emission did not arise from this source, but it was emission from the star-forming region W49A (Suárez et al., in prep.), located ∼11′ away, which spilled into the sidelobes of the single-dish telescope. We believe that the detection reported by Yoon et al. (2014) toward IRAS 19071+0857 is likewise contaminated by W49A.

In what follows we discuss the individual sources where H_2O maser emission is detected. The spectra observed toward these sources are shown in Fig. 1, while the main parameters of the H_2O masers are listed in Table 2.

4.1. IRAS 13483−5905

The nature of this source is still unclear. The similar fluxes in the IR between the 2MASS data (Ramos-Larios et al. 2009) and the observations in Ramos-Larios et al. (2012), should suggest a post-AGB nature. Ramos-Larios et al. (2009) report an optical counterpart for this source. However, it is possible that the optical/near-IR source is not the same as the mid/far-IR one. The position given by Ramos-Larios et al. (2009) corresponds to the near-IR source 2MASS J13514373-5920155. On the other hand, the WISE data catalog report a mid-IR source, WISE J135144.47-592016.7, which is ≃5.9″ away from the near-IR position. On close inspection of the WISE images, we could see that the position reported WISE J135144.47-592016.7 corresponds to a strong source seen in the bands at 4.6, 12, and 22 μm, but there is a source at 3.4 μm whose position matches

that of 2MASS J13514373-5920155. Therefore, it seems that there are two different nearby sources, and the source seen at $\lambda \geq 4.6\,\mu$m is an optically obscured source that also corresponds to IRAS 13483−5905. This is the most likely source associated to the water maser emission. We note that te Lintel Hekkert et al. (1991) reported non-detection of OH masers toward IRAS 13483−5905.

The H_2O spectrum shows at least ten different components, which seem to cluster into two groups. The blueshifted group comprises the components at V_{LSR} = −27.8, −21.9, −18.4, −15.2, −13.9, −6.3 km s^{-1}, while the redshifted one is composed of components at V_{LSR} = 15.2, 18.5, 24.0, and 28.7 km s^{-1}. If we interpret each group as arising from opposite sides of the expanding envelope, the mean velocity of each group would be ≃−20.85 and 21.95 km s^{-1}, so the stellar velocity is ≃0.55 km s^{-1}. However, the total velocity spread of the H_2O maser components (≃56 km s^{-1}) would imply an expansion velocity of ≃28 km s^{-1}, which is relatively high for an expanding envelope around an AGB or post-AGB star (see Sect. 1). Interferometric observations would be needed to ascertain the nature of the structure traced by this H_2O maser emission.

4.2. IRAS 14249−5310

Ramos-Larios et al. (2009) report the absence of an optical counterpart for this source. The observations by Ramos-Larios et al. (2012) show a point source in the near-IR. The comparison of infrared fluxes in different epochs (Fouque et al. 1992; Ramos-Larios et al. 2012) shows a difference, with the source being brighter (by 1.65, 1.01, and 0.17 mag in J, H, and K bands, respectively) in the more recent observations. The 2MASS image shown in Ramos-Larios et al. (2009) has a lower angular resolution, and it is not able to resolve the object from another nearby one, so it cannot be used to compare the source flux with the other two epochs. The flux variation with time suggests that IRAS 14249−5310 may be an AGB star. This source does not show any detectable OH maser emission (te Lintel Hekkert et al. 1991; Silva et al. 1993).

Our water maser spectrum shows at least two components at −19.8 and −10.1 km s^{-1}. There are hints of other possible components between 30 and 50 km s^{-1}, but it is not possible to confirm them with these data.

4.3. IRAS 15408−5413

This source has no optical counterpart (Ramos-Larios et al. 2009). It shows variability in its near-IR emission of at least 0.8 mag in K and 0.2 in L' (see the different photometric measurements in Epchtein et al. 1987; Le Bertre et al. 1988; Le Bertre & Nyman 1990; Le Bertre 1993; Garcia-Lario et al. 1997; Ramos-Larios et al. 2009). However, its light curve does not show the periodic variability typical of OH/IR (AGB) stars (Le Bertre 1993). It has been suggested that the source might be a supergiant (Le Bertre & Nyman 1990; Le Bertre 1993) or a "born again" AGB star (Le Bertre et al. 1988), although these classifications are uncertain. In any case, its IR variability seems to rule out a post-AGB or PN nature.

Te Lintel Hekkert et al. (1991) detected OH emission, with several components in emission and absorption. However, the spectrum does not show the typical double-peaked profile of OH masers in AGB stars. The OH emission may arise from more than one source within their beam or, alternatively, trace independent episodes of mass loss. There is also SiO maser emission (Le Bertre & Nyman 1990), whose spectrum shows a wide (12.2 km s^{-1} width) and irregular profile, apparently due to the blending of several velocity components, with centroid LSR velocity of −83.6 km s^{-1}.

Deguchi et al. (1989) failed to detect H_2O maser emission with Parkes, reaching an rms = 0.5 Jy. Our spectrum (with an rms noise of 0.09 Jy) shows an asymmetric double-peaked profile, with components at −82.6 and −76.3 km s^{-1}. The velocity of the stronger component is close to the SiO centroid velocity, while that of the secondary peak is outside the bulk of SiO emission. Since SiO emission tends to be close to the stellar velocity, the stronger H_2O component seems to trace gas at this stellar velocity, while the secondary component might trace the receding part of the envelope. Both SiO and H_2O components are within the velocity range of OH maser emission. The flux density of 53 Jy we obtained should have been detected by Deguchi et al. (1989), which indicates a strong variability of the water maser emission in this source.

4.4. IRAS 15452−5459

This object is a post-AGB star with an hour-glass shape in infrared images (Sahai et al. 2007; Ramos-Larios et al. 2012). Maser emission of SiO, OH, and H_2O has been previously detected toward it (te Lintel Hekkert et al. 1991; Caswell 1998; Deacon et al. 2004; Deacon et al. 2007; Cerrigone et al. 2013).

The spectral shape of the H_2O maser has changed. While Deacon et al. (2007) show an irregular profile, our spectrum and the profile in Cerrigone et al. (2013), both taken at later epochs, tend to cluster in two groups of features, resembling a more regular double-peaked profile. The interferometric SiO, H_2O, and OH maser observations by Cerrigone et al. (2013) show different spatio-kinematical patterns in these species. While OH masers seem to trace outflows along the lobes of the nebula, the SiO and H_2O maser components display a velocity gradient perpendicular to it, which could be tracing rotational motions in a circumstellar torus.

4.5. IRAS 17021−3109

This is a heavily obscured object (Ramos-Larios et al. 2012) with no optical counterpart (Ramos-Larios et al. 2009). The near-IR fluxes of the most likely counterpart for the IRAS sources are similar in different epochs (Ramos-Larios et al. 2009, 2012), suggesting a post-AGB nature. We note that Garcia-Lario et al. (1997) report brighter magnitudes, but they might correspond to a different object in the field.

The spectrum of OH maser emission at 1612 MHz (David et al. 1993a) shows at least four peaks between ∼−30.5 and −5.5 km s^{-1}. OH emission at 1667 MHz has also been detected (David et al. 1993b), with a single peak at −7.5 km s^{-1}.

Our H_2O maser spectrum shows a single peak at +13.5 km s^{-1}. It lies well outside the velocity range of the OH emission. Therefore, it is possible that OH and H_2O masers arise from different nearby sources but with a velocity difference between them of ∼30 km s^{-1}. Alternatively, if the emission from both maser species arises from the same source, it would indicate the presence of non-spherical mass loss.

4.6. IRAS 17291−2147

This source has a weak optical counterpart (Ramos-Larios et al. 2009). Its near-IR fluxes are similar in different epochs (Ramos-Larios et al. 2009, 2012), which suggests a post-AGB nature. No OH maser emission has been detected toward this source (te Lintel Hekkert et al. 1991).

Yoon et al. (2014) report the presence of H_2O maser emission, with only one velocity component at $V_{LSR} = -16.3$ km s^{-1} having been clearly detected. Our Robledo spectrum resolves two spectral components around that velocity. However, the GBT spectrum, with a much higher signal-to-noise ratio, shows at least four components, at −27.0, −16.1, −14.5, and +69.1 km s^{-1}. Other possible weaker components might be present, but we cannot confirm them at this stage. The total velocity spread of the H_2O maser components is large, ≃96 km s^{-1}. This means that IRAS 17291−2147 is a candidate water fountain source. Its confirmation as such would require interferometric observations to ascertain that all velocity components observed with single-dish arise from the same source.

4.7. IRAS 17348−2906

This object has an optical counterpart (Ramos-Larios et al. 2009). The near-IR fluxes in the observations of Garcia-Lario et al. (1997) are similar to those in 2MASS data (Ramos-Larios et al. 2009), suggesting it is a post-AGB star.

OH maser emission has been reported in this source, between ∼8 and 13 km s^{-1} (te Lintel Hekkert et al. 1991; David et al. 1993a). Our H_2O maser spectrum shows at least three components: two narrow ones at ≃1.0, 2.6 km s^{-1} and a wider one between 6 and 9 km s^{-1}, which could be the blending of several unresolved ones. Most of the H_2O maser emission lies outside the velocity range of OH maser emission, so it is unclear whether this indicates non-spherical mass loss or if the emission from both molecules arises from different sources.

4.8. IRAS 17393−2727 (OH 0.9+1.3)

This source shows a bipolar morphology in the optical (Manteiga et al. 2011), and its IR colors suggest that the central star is strongly obscured (Ramos-Larios et al. 2012). The presence of bright [Ne II] emission indicates that it is a planetary nebula (García-Hernández et al. 2007).

IRAS 17393−2727 presents both OH maser (Zijlstra et al. 1989; Sevenster et al. 1997) and radio continuum emission (Pottasch et al. 1987), whose spatial association have been confirmed with interferometric observations, making it one of the six confirmed planetary nebulae with OH emission (Uscanga et al. 2012). The OH spectrum at 1612 MHz shows two peaks located at $V_{LSR} = -122.8$ and −93 km s^{-1}.

Previous observations of water maser emission toward this source resulted in non-detections (Gómez et al. 1990; Deacon et al. 2007; Yoon et al. 2014). However, we detected water maser emission with a single component of ≃1 Jy at $V_{LSR} = -107.6$ km s^{-1}, above the detection threshold of Deacon et al. (2007) and Yoon et al. (2014). Although with our single-dish observations we cannot determine whether the water maser emission is associated with IRAS 17393−2727, the velocity of the observed component is very close to the mean velocity of the OH peaks (∼−107.9 km s^{-1}), which is the expected central velocity of the star. This would be a very unlikely coincidence if the water maser emission arises from a different source. Therefore, we think this is a most probable candidate to also be a water-maser-emitting PN. The presence of both OH and H_2O emission and its strong obscuration make it a PN very similar to K 3−35 (Miranda et al. 2001), IRAS 17347−3139 (de Gregorio-Monsalvo et al. 2004), and IRAS 16333−4807 (Uscanga et al. 2014) and, like them, an extremely young PN.

4.9. IRAS 18039−1903

This source does not have an optical counterpart, and it is very weak in the near-IR (Ramos-Larios et al. 2012). Its infrared colors confirm that it is a heavily obscured object (Ramos-Larios et al. 2012).

OH maser emission has been detected in this source (te Lintel Hekkert et al. 1991; David et al. 1993a,b), showing a double-peaked profile characteristic of OH/IR stars, with LSR velocities ≃143.3 and 170.1 km s^{-1}. H_2O maser emission has been detected by Yoon et al. (2014), with two distinct velocity components. Our spectrum is similar, but it shows four components at 153.1, 162.0, 162.9, and 165.2 km s^{-1}. The peak emission is slightly blueshifted with respect to the stellar velocity inferred from the OH spectrum (≃157.6 km s^{-1}), while the other three are redshifted. All H_2O maser components are within the velocity range of the OH emission.

4.10. IRAS 18113−2503

The observations presented here yielded the first detection of water maser emission toward this source, although interferometric follow-up observations have already been reported in Gómez et al. (2011). That paper describes the source in detail. As mentioned there, it seems to be a post-AGB star. The water maser spectrum shows a wealth of components, spanning an extremely wide velocity range of ≃500 km s^{-1}. This is the water fountain with the fastest jet known to date.

4.11. IRAS 18361−1203

This source has a weak optical counterpart in red DSS plates, and its infrared fluxes do not seem to vary significantly (Ramos-Larios et al. 2009, 2012), which suggests this is a post-AGB star. IRAS 18361−1203 shows a double-peaked profile in OH (te Lintel Hekkert et al. 1991; David et al. 1993a) with velocities ∼11.77 and 19.32 km s^{-1}.

Yoon et al. (2014) report a non-detection of water maser emission, with a 3σ upper limit of ∼1.3 Jy. Our spectrum shows weak emission, well below their detection limit, with a single confirmed component at ≃12.7 km s^{-1}.

4.12. IRAS 18596+0315 (OH 37.1-0.8)

This object is weak in the near-IR, and it has infrared colors that indicate strong obscuration (Ramos-Larios et al. 2012). OH maser emission is present in this source and shows a double-peaked profile with ∼28 km s^{-1} separation between them (Winnberg et al. 1975; Bowers 1978; Baud et al. 1985; Herman & Habing 1985; Herman et al. 1985; Chengalur et al. 1993; Gómez et al. 1994; Sevenster et al. 2001; Szymczak & Gérard 2004; Engels & Jiménez-Esteban 2007). The OH central velocity is close to that of the CO emission (Rizzo et al. 2013). OH maser emission at 1665 and 1667 MHz (Dickinson & Turner 1991; Lewis 1997; Szymczak & Gérard 2004) extends beyond the velocity range of the emission at 1612 MHz.

Interferometric observations of OH (Baud et al. 1985; Herman et al. 1985; Gómez et al. 1994; Gómez & Rodríguez 2000; Sevenster et al. 2001; Amiri et al. 2011) show that the two peaks are actually the blend of different features. Blue- and redshifted groups are spatially separated by ∼150 mas along the E-W direction. It is unclear whether OH emission arises from a biconical or an equatorial flow. Jewell et al. (1991) reported a tentative detection of SiO, but it has not been confirmed in subsequent observations (Deguchi et al. 2004).

Water maser emission has been previously detected in this source (Engels et al. 1986; Brand et al. 1994; Gómez et al. 1994; Engels 2002; Deacon et al. 2007), showing a variable spectral pattern of multiple components, extending over a range ~57 km s^{-1}, beyond the velocity range of OH. This strongly suggests it is a water fountain, although there is no published map showing that the water maser emission traces a jet. Gómez et al. (1994) proved that OH and water maser emission arise from the same source, confirming that the latter lies outside the velocity range of the former, but they could not determine the spatial distribution of the water masers or even confirm that all the maser emission detected with single dish actually arise from this source, since their interferometric observation only showed a single peak of water maser emission at $V_{\rm LSR} \simeq 65.7$ km s^{-1}. Our single-dish data also shows a single component, at $V_{\rm LSR} \simeq 61.6$ km s^{-1}.

4.13. IRAS 19134+2131

This is a confirmed water fountain, and the only one in which OH emission has not been detected, despite several searches (Lewis et al. 1987; Hu et al. 1994; Likkel 1989).

Water maser emission was first detected in this source by Engels et al. (1984), who identified a wide velocity spread (~110 km s^{-1}) in their components. The water maser emission traces a collimated jet (Imai et al. 2004, 2007). Our spectrum shows five distinct components spanning a range of ≃115 km s^{-1}.

4.14. IRAS 19190+1102

This object is a known water fountain, which was first detected by Likkel (1989), who obtained a water maser spectrum with a wide velocity range of ≥70 km s^{-1}, well outside the velocity range covered by the OH maser emission. The distribution and proper motions of the H_2O maser emission (Day et al. 2010) confirms that it arises from a collimated jet. The departure of the OH spectrum from the typical double-peaked profile in OH/IR stars (Likkel 1989) suggests that this object is already in the post-AGB phase.

Our water maser spectrum shows components spanning ~143 km s^{-1}. We note that this velocity range is slightly more than found by Day et al. (2010). In particular, our components with the most extreme velocities (−55.0 and +87.9 km s^{-1}) were not present in their spectra, although they were above their sensitivity limit. While the appearance of these new components could merely be the result of the typical variability of water masers, it might also indicate an acceleration process in the jet.

4.15. IRAS 19319+2214

This is an optically obscured source, with a relatively constant near-IR flux (Ramos-Larios et al. 2009, 2012), which suggests it is a post-AGB star.

It shows a double-peaked OH spectrum (Lewis et al. 1990; David et al. 1993a), with components at ~12 and 29 km s^{-1}. Water maser emission, spanning a velocity range of ≃12 km s^{-1}, was first detected by Engels & Lewis (1996). Our GBT water maser spectrum shows five components over a wider velocity spread (~20 km s^{-1}), whose most extreme velocities are similar to those seen in OH.

5. Discussion and conclusions

The detection rate of water masers seems to be higher in obscured objects (7% and 14% in objects with and without an optical counterpart, respectively). This is consistent with our results in previous surveys (Suárez et al. 2007, 2009). Another significant trend in our data is the high detection rate of water masers in bipolar objects. Out of the seven sources in our sample that are clearly bipolar in the near-IR (Ramos-Larios et al. 2012), we detected water maser emission in three. This high detection rate (43%) clearly suggests that water maser emission tends to be associated with collimated mass-loss processes, either directly (tracing jets, as in water fountains) or indirectly (tracing toroidal structures perpendicular to the bipolar nebulae). However, all these detection rates should be taken with care, since the sensitivity of our observations is not homogeneous throughout the sample.

We have identified a water fountain candidate (IRAS 17291−2147) with a total velocity spread of ~96 km s^{-1} in its water maser components. Another two sources (IRAS 17021−3109 and IRAS 17348−2906) show water maser emission whose velocity lies outside the velocity range covered by OH masers, a criterion that is also used to identify water fountain candidates. IRAS 17291−2147, however, has a very scarce number of maser components, as in the case of IRAS 19134+2131 or IRAS 18596+0315. The spectrum of these water fountain candidates is strikingly different from those of IRAS 18113−2503 or IRAS 19190+1102, which are very rich in maser components. This suggests an intrinsically different nature of these sources, although they are collectively included in the "water fountain" category based on the wide velocity spread of their masers. Also, IRAS 17291−2147 qualifies as a water fountain candidate, because of the detection of a very weak component at ~69 km s^{-1}, which was below the sensitivity of previous observations. Moreover, given the high variability of water maser emission, components at extreme velocities may be above or below the sensitivity of the telescope depending on the epoch of observation.

If the identification of a source as a water fountain depends so much on the sensitivity or the epoch of the observations, there is thus an observational bias in the definition of this type of source. In fact, post-AGB stars have high-velocity winds of several hundred km s^{-1}, as seen in optical and infrared data (e.g., Riera et al. 1995; Witt et al. 2009; Sánchez Contreras et al. 2010), so the presence of these velocities in their maser spectra should not be surprising. It is possible that most water-maser-emitting post-AGBs will show high-velocity maser components when observed with high enough sensitivity or if monitored for a long enough time. Also, a particular orientation (close to the plane of the sky) of the jets traced by water masers could make components with intrinsically high velocities not appear as such in a spectrum. Therefore, high-velocity jets traced by water masers could be much more widespread in post-AGB stars than previously thought. If this were the case, the segregation of a group of water-maser-emitting post-AGBs as "water fountains", based only on the velocity spread of the masers, would lose its meaning to a certain extent. We think it would be interesting to further differentiate those "water fountains" with high maser luminosities as a special group. This spectral characteristic could be due to a higher mass in their progenitor or to their being in a different evolutionary stage. Monitoring of the water maser spectra of "water fountains" or a better characterization of their stellar properties would shed some light on the origin of these spectral differences.

We also identified IRAS 17393−2727 as a possible new H_2O-PN. This is the sixth source that could pertain to this category. This PN also shows OH emission. The PNe K3-35 and IRAS 17347−3139 also show maser emission from both

molecules. PN emitting OH and/or H_2O masers are supposed to be very young PNe. In fact, most of them are optically obscured and spatially compact, with the exception of the NGC 6302 (an OHPN) and IRAS 18061−2505 (Suárez et al. 2006), which show extended optical emission. These two sources only show maser emission from one of the species (OH in NGC 6302 and H_2O in IRAS 18061−2505), while observations of the other yielded negative results (Deacon et al. 2007; Gómez et al. 2008). We suggest that the presence of both maser species in a PN is a better tracer of its youth, rather than the presence of just one of them.

Interferometric observations will be needed to confirm the nature of IRAS 17291–2147, IRAS 17021–3109, and IRAS 17348–2906 as water fountains, and of IRAS 17393−2727 as an H_2O-PN. These observations will indicate whether all maser components arise from these evolved objects.

Acknowledgements. This work is partially based on observations carried out at MDSCC (Robledo), under the Host Country Radio Astronomy program. The Parkes radio telescope is part of the Australia Telescope National Facility, which is funded by the Commonwealth of Australia for operation as a National Facility managed by CSIRO. The National Radio Astronomy Observatory is a facility of the National Science Foundation operated under cooperative agreement by Associated Universities, Inc. J.F.G., O.S., L.F.M., and J.M.T. are supported by MICINN (Spain) grants AYA2011-30228-C03 and AYA2014-57369-C3, while MAG is supported by grant AYA2011-29754-C03-02 (all these grants include FEDER funds). J.R.R. acknowledges support from MICINN grants AYA2009-07304 and AYA2012-32032. A.P. acknowledges the financial support from UNAM and CONACyT, México. G.R.L. acknowledges support from CONACyT and PROMEP (Mexico).

References

Amiri, N., Vlemmings, W., & van Langevelde, H. J. 2011, A&A, 532, A149
Baud, B., Sargent, A. I., Werner, M. W., & Bentley, A. F. 1985, ApJ, 292, 628
Bowers, P. F. 1978, A&A, 64, 307
Blöcker, T. 1995a, A&A, 297, 727
Blöcker, T. 1995b, A&A, 299, 755
Brand, J., Cesaroni, R., Caselli, P., et al. 1994, A&AS, 103, 541
Caswell, J. L. 1998, MNRAS, 297, 215
Cerrigone, L., Menten, K. M., & Wiesemeyer, H. 2013, MNRAS, 434, 542
Cesaroni, R., Palagi, F., Felli, M., et al. 1988, A&AS, 76, 445
Chengalur, J. N., Lewis, B. M., Eder, J., & Terzian, Y. 1993, ApJS, 89, 189
Comoretto, G., Palagi, F., Cesaroni, R., et al. 1990, A&AS, 84, 179
David, P., Le Squeren, A. M., & Sivagnanam, P. 1993a, A&A, 277, 453
David, P., Le Squeren, A. M., Sivagnanam, P., & Braz, M. A. 1993b, A&AS, 98, 245
Day, F. M., Pihlström, Y. M., Claussen, M. J., & Sahai, R. 2010, ApJ, 713, 986
Deacon, R. M., Chapman, J. M., & Green, A. J. 2004, ApJS, 155, 595
Deacon, R. M., Chapman, J. M., Green, A. J., & Sevenster, M. N. 2007, ApJ, 658, 1096
de Gregorio-Monsalvo, I., Gómez, Y., Anglada, G., et al. 2004, ApJ, 601, 921
Deguchi, S., Nakada, Y., & Forster, J. R. 1989, MNRAS, 239, 825
Deguchi, S., Fujii, T., Glass, I. S., et al. 2004, PASJ, 56, 765
Dickinson, D. F., & Turner, B. E. 1991, ApJS, 75, 1323
Engels, D. 2002, A&A, 388, 252
Engels, D., & Jiménez-Esteban, F. 2007, A&A, 475, 941
Engels, D., & Lewis, B. M. 1996, A&AS, 116, 117
Engels, D., Habing, H. J., Olnon, F. M., Schmid-Burgk, J., & Walmsley, C. M. 1984, A&A, 140, L9
Engels, D., Schmid-Burgk, J., & Walmsley, C. M. 1986, A&A, 167, 129
Engels, D., Schmid-Burgk, J., & Walmsley, C. M. 1988, A&A, 191, 283
Epchtein, N., Le Bertre, T., Lepine, J. R. D., et al. 1987, A&AS, 71, 39
Fouque, P., Le Bertre, T., Epchtein, N., Guglielmo, F., & Kerschbaum, F. 1992, A&AS, 93, 151
García-Hernández, D. A., Perea-Calderón, J. V., Bobrowsky, M., & García-Lario, P. 2007, ApJ, 666, L33
Garcia-Lario, P., Manchado, A., Pych, W., & Pottasch, S. R. 1997, A&AS, 126, 479
Gómez, Y., & Rodríguez, L. F. 2000, in Asymmetrical Planetary Nebulae II: From Origins to Microstructures, eds. J. H. Kastner, N. Soker, & S. A. Rappaport, (San Francisco: ASP), ASP Conf. Ser., 199, 75
Gómez, Y., Moran, J. M., & Rodríguez, L. F. 1990, Rev. Mex. Astron. Astrofis., 20, 55
Gómez, Y., Rodríguez, L. F., Contreras, M. E., & Moran, J. M. 1994, Rev. Mex. Astron. Astrofis., 28, 97
Gómez, J. F., Suárez, O., Gómez, Y., et al. 2008, AJ, 135, 2074
Gómez, J. F., Rizzo, J. R., Suárez, O., et al. 2011, ApJ, 739, L14
Gómez, J. F., Uscanga, L., Suárez, O., Rizzo, J. R., & de Gregorio-Monsalvo, I. 2014, Rev. Mex. Astron. Astrofis., 50, 137
Gómez, J. F., Suárez, O., Bendjoya, P., et al. 2015a, ApJ, 799, 186
Gómez, J. F., Uscanga, L., & Suárez, O. 2015b, in 20.DA.10 Research and Teaching in Astrophysics in Guanajuato, eds. M. T. Trinidad, H. Andernach, & M. Avalos (Guanajuato: Univ. Guanajuato), in press
Han, F., Mao, R. Q., Lu, J., et al. 1998, A&AS, 127, 181
Herman, J., & Habing, H. J. 1985, A&AS, 59, 523
Herman, J., Baud, B., Habing, H. J., & Winnberg, A. 1985, A&A, 143, 122
Hu, J. Y., te Lintel Hekkert, P., Slijkhuis, F., et al. 1994, A&AS, 103, 301
Imai, H. 2007, in Astrophysical Masers and Their Environments, eds. J. M. Chapman, & W. A. Baan (Cambridge: Cambridge Univ. Press), IAU Symp., 242, 279
Imai, H., Morris, M., Sahai, R., Hachisuka, K., & Azzollini, F. J. R. 2004, A&A, 420, 265
Imai, H., Sahai, R., & Morris, M. 2007, ApJ, 669, 424
Jewell, P. R., Snyder, L. E., Walmsley, C. M., Wilson, T. L., & Gensheimer, P. D. 1991, A&A, 242, 211
Le Bertre, T. 1993, A&AS, 97, 729
Le Bertre, T., & Nyman, L.-A. 1990, A&A, 233, 477
Le Bertre, T., Heydari-Malayeri, M., & Epchtein, N. 1988, A&A, 197, 143
Lewis, B. M. 1989, ApJ, 338, 234
Lewis, B. M. 1997, ApJS, 109, 489
Lewis, B. M., & Engels, D. 1988, Nature, 332, 49
Lewis, B. M., Eder, J., & Terzian, Y. 1987, AJ, 94, 1025
Lewis, B. M., Eder, J., & Terzian, Y. 1990, ApJ, 362, 634
Likkel, L. 1989, ApJ, 344, 350
Likkel, L., Morris, M., & Maddalena, R. J. 1992, A&A, 256, 581
Manteiga, M., García-Hernández, D. A., Ulla, A., Manchado, A., & García-Lario, P. 2011, AJ, 141, 80
Migenes, V., Horiuchi, S., Slysh, V. I., et al. 1999, ApJS, 123, 487
Miranda, L. F., Gómez, Y., Anglada, G., & Torrelles, J. M. 2001, Nature, 414, 284
Pottasch, S. R., Bignell, C., & Zijlstra, A. 1987, A&A, 177, L49
Ramos-Larios, G., Guerrero, M. A., Suárez, O., Miranda, L. F., & Gómez, J. F. 2009, A&A, 501, 1207
Ramos-Larios, G., Guerrero, M. A., Suárez, O., Miranda, L. F., & Gómez, J. F. 2012, A&A, 545, A20
Reid, M. J., & Moran, J. M. 1981, ARA&A, 19, 231
Reid, M. J., Muhleman, D. O., Moran, J. M., Johnston, K. J., & Schwartz, P. R. 1977, ApJ, 214, 60
Riera, A., García-Lario, P., Manchado, A., Pottasch, S. R., & Raga, A. C. 1995, A&A, 302, 137
Rizzo, J. R., Gómez, J. F., Miranda, L. F., et al. 2013, A&A, 560, A82
Sahai, R., Morris, M., Sánchez Contreras, C., & Claussen, M. 2007, AJ, 134, 2200
Sánchez Contreras, C., Cortijo-Ferrero, C., Miranda, L. F., Castro-Carrizo, A., & Bujarrabal, V. 2010, ApJ, 715, 143
Sevenster, M. N., Chapman, J. M., Habing, H. J., Killeen, N. E. B., & Lindqvist, M. 1997, A&AS, 122, 79
Sevenster, M. N., van Langevelde, H. J., Moody, R. A., et al. 2001, A&A, 366, 481
Silva, A. M., Azcarate, I. N., Poppel, W. G. L., & Likkel, L. 1993, A&A, 275, 510
Suárez, O., García-Lario, P., Manchado, A., et al. 2006, A&A, 458, 173
Suárez, O., Gómez, J. F., & Morata, O. 2007, A&A, 467, 1085
Suárez, O., Gómez, J. F., Miranda, L. F., et al. 2009, A&A, 505, 217
Szymczak, M., & Gérard, E. 2004, A&A, 423, 209
te Lintel Hekkert, P., Caswell, J. L., Habing, H. J., et al. 1991, A&AS, 90, 327
Uscanga, L., Gómez, J. F., Suárez, O., & Miranda, L. F. 2012, A&A, 547, A40
Uscanga, L., Gómez, J. F., Miranda, L. F., et al. 2014, MNRAS, 444, 217
Vassiliadis, E., & Wood, P. R. 1993, ApJ, 413, 641
Vassiliadis, E., & Wood, P. R. 1994, ApJS, 92, 125
Winnberg, A., Nguyen-Quang-Rieu, Johansson, L. E. B., & Goss, W. M. 1975, A&A, 38, 145
Witt, A. N., Vijh, U. P., Hobbs, L. M., et al. 2009, ApJ, 693, 1946
Yoon, D.-H., Cho, S.-H., Kim, J., Yun, Y. J., & Park, Y.-S. 2014, ApJS, 211, 15
Yung, B. H. K., Nakashima, J.-I., Imai, H., et al. 2013, ApJ, 769, 20
Zijlstra, A. A., te Lintel Hekkert, P., Pottasch, S. R., et al. 1989, A&A, 217, 157
Zuckerman, B., & Lo, K. Y. 1987, A&A, 173, 263

Pages 8 to 15 are available in the electronic edition of the journal at http://www.aanda.org

Table 1. Observed sources.

IRAS name	RA (J2000)	Dec (J2000)	Observation date	Telescope[a]	rms[b] (Jy)	Previous[c] (Jy)	References[d]	Image[e]
07582−4059	07 59 57.7	−41 07 23	14-Sep-2008	PKS	0.16			V
08143−4406	08 16 03.0	−44 16 04	14-Sep-2008	PKS	0.18			V
08213−3857	08 23 12.1	−39 07 08	14-Sep-2008	PKS	0.12			V
09055−4629	09 07 19.5	−46 41 23	12-Sep-2008	PKS	0.09			N
09102−5101	09 11 57.3	−51 14 24	12-Sep-2008	PKS	0.06			V
			14-Sep-2008	PKS	0.08			
09119−5150	09 13 33.0	−52 02 41	14-Sep-2008	PKS	0.09			V
09362−5413	09 37 51.8	−54 27 09	14-Sep-2008	PKS	0.11			V
09378−5117	09 39 37.0	−51 31 29	14-Sep-2008	PKS	0.08			V
10194−5625	10 21 15.2	−56 40 32	14-Sep-2008	PKS	0.09			N, O
11444−6150	11 46 54.0	−62 07 09	13-Sep-2008	PKS	0.07			N, O
11488−6432	11 51 17.3	−64 49 12	12-Sep-2008	PKS	0.11			V
11544−6408	11 56 57.8	−64 25 17	12-Sep-2008	PKS	0.08			V
11549−6225	11 57 30.8	−62 42 12	12-Sep-2008	PKS	0.08			N, O
12067−4508	12 09 23.8	−45 25 35	15-Sep-2008	PKS	0.13	<1.2	1	V
12302−6317	12 33 07.0	−63 33 43	15-Sep-2008	PKS	0.12	<0.7	2	V
12360−5740	12 38 53.1	−57 56 31	13-Sep-2008	PKS	0.10			V
13010−6012	13 04 05.5	−60 28 46	14-Sep-2008	PKS	0.16			V
13245−5036	13 27 36.1	−50 52 06	14-Sep-2008	PKS	0.15			V
13266−5551	13 29 51.0	−56 06 54	14-Sep-2008	PKS	0.15			V
13313−5838	13 34 37.4	−58 53 32	14-Sep-2008	PKS	0.15			V
13398−5951	13 43 12.5	−60 07 03	12-Sep-2008	PKS	0.12			N
13404−6059	13 43 50.3	−61 14 30	13-Sep-2008	PKS	0.10			N, O
13421−6125	13 45 34.0	−61 40 03	13-Sep-2008	PKS	0.09			V
13428−6232	13 46 20.5	−62 48 00	15-Sep-2008	PKS	0.13			V
13483−5905	13 51 43.7	−59 20 15	13-Sep-2008	PKS	0.09			V
14104−5819	14 14 00.5	−58 33 58	13-Sep-2008	PKS	0.09			N, O
14249−5310	14 28 24.7	−53 24 04	13-Sep-2008	PKS	0.07			N
14325−6428	14 36 34.4	−64 41 31	15-Sep-2008	PKS	0.23			V
14331−6435	14 37 10.1	−64 48 05	15-Sep-2008	PKS	0.15			V
14346−5952	14 38 24.6	−60 04 53	15-Sep-2008	PKS	0.14			V
14429−4539	14 46 13.8	−45 52 05	15-Sep-2008	PKS	0.14			V
14521−5300	14 55 45.7	−53 12 30	15-Sep-2008	PKS	0.07			V
15038−5533	15 07 34.7	−55 44 50	15-Sep-2008	PKS	0.09			N
15229−5433	15 26 40.5	−54 44 17	12-Sep-2008	PKS	0.08			V
15284−6026	15 32 37.1	−60 37 04	15-Sep-2008	PKS	0.08			N, O
15408−5413	15 44 39.8	−54 23 05	15-Sep-2008	PKS	0.09			N, O
15408−5657	15 44 48.3	−57 07 08	15-Sep-2008	PKS	0.09	<1.5	1	N
15452−5459	15 49 11.3	−55 08 51	12-Sep-2008	PKS	0.08	6.5 ± 0.3	3, 4	N
15531−5704	15 57 10.9	−57 13 21	12-Sep-2008	PKS	0.09			N, O
16206−5956	16 25 02.6	−60 03 32	14-Sep-2008	PKS	0.17			V
16209−4714	16 24 33.9	−47 21 30	12-Sep-2008	PKS	0.08	<0.4	3	V
16245−3859	16 27 53.7	−39 05 46	12-Sep-2008	PKS	0.11			N, O
16279−4757	16 31 38.7	−48 04 06	14-Sep-2008	PKS	0.12			V
16296−4507	16 33 12.5	−45 13 43	12-Sep-2008	PKS	0.08			V
16279−8158	16 37 51.6	−82 04 49	12-Sep-2008	PKS	0.09			V
16507−4810	16 54 30.9	−48 15 24	12-Sep-2008	PKS	0.09	<0.4	3	V

Notes. [a] GBT: Green Bank. PKS: Parkes. ROB: Robledo. VLA: Very Large Array. [b] One-sigma noise level per spectral channel. [c] Previous water maser observations of the sources reported in the literature. For detections, we give the highest reported flux density and its 2σ uncertainty. For non-detections, the lowest reported 3σ upper limit is given. [d] References for previous water maser observations. [e] Visibility of sources in optical and infrared images. V: sources with optical counterpart in the Digital Sky Survey (as mentioned in Ramos-Larios et al. 2009, 2012), or with optical spectrum in Suárez et al. (2006). N: sources detected only at near-infrared wavelenghts or longer (Ramos-Larios et al. 2009, 2012). M: sources detected only at mid-infared wavelenghts or longer (Ramos-Larios et al. 2009, 2012). O: sources with strong obscuration, based on their infrared colours (Table 9 in Ramos-Larios et al. 2012). [f] Migenes et al. (1999) reported a water maser of 56 Jy, which was incorrectly labelled as IRAS 18434−0042. The maser is $\simeq 2^\circ$ away from this infrared source and it is associated with the star-forming region W43S instead. [g] We observed IRAS 19071+0857 with Robledo and GBT, but it was contaminated by the strong maser emission from W49A, which spilled into the telescope sidelobes. The reported detection by Yoon et al. (2014) is also most likely contaminated. The upper limit listed in this table corresponds to observations taken with the Very Large Array (Suárez et al., in prep.), which confirmed that the maser emission was not associated with IRAS 19071+0857. [h] Labeled as 19375+2359 in Han et al. (1998).

References. (1) Deguchi et al. (1989); (2) Suárez et al. (2009); (3) Deacon et al. (2007); (4) Cerrigone et al. (2013); (5) Yoon et al. (2014); (6) Gómez et al. (1990); (7) Suárez et al. (2007); (8) Gómez et al. (2011); (9) Engels et al. (1986); (10) Yung et al. (2013); (11) Brand et al. (1994); (12) Gómez et al. (1994); (13) Engels (2002); (14) Likkel (1989); (15) Engels et al. (1984); (16) Likkel et al. (1992); (17) Comoretto et al. (1990); (18) Imai et al. (2004); (19) Imai et al. (2007); (20) Engels & Lewis (1996); (21) Likkel (1989); (22) Day et al. (2010); (23) Han et al. (1998); (24) Zuckerman & Lo (1987).

Table 1. continued.

IRAS name	RA (J2000)	Dec (J2000)	Observation date	Telescope[a]	rms[b] (Jy)	Previous[c] (Jy)	References[d]	Image[e]
16517−3626	16 55 06.2	−36 31 32	12-Sep-2008	PKS	0.09			V
16558−3417	16 59 10.5	−34 22 05	12-Sep-2008	PKS	0.08			M
16567−3838	17 00 09.0	−38 43 09	15-Sep-2008	PKS	0.10			N, O
17021−3109	17 05 23.3	−31 13 18	05-Jun-2008	ROB	0.14			N, O
			21-Mar-2010	GBT	0.022			
17021−3054	17 05 24.1	−30 58 14	06-Jun-2008	ROB	0.10			N
			21-Mar-2010	GBT	0.022			
17052−3245	17 08 33.2	−32 49 44	13-Sep-2008	PKS	0.10			N, O
17067−3759	17 10 08.3	−38 03 22	13-Sep-2008	PKS	0.09			N
17097−3624	17 13 05.1	−36 27 53	13-Sep-2008	PKS	0.14	<0.4	3	N, O
17149−3053	17 18 10.9	−30 56 39	12-Sep-2008	PKS	0.08	<0.9	5	N
			03-Mar-2010	GBT	0.023			
17150−3224	17 18 19.8	−32 27 21	12-Sep-2008	PKS	0.08	<0.4	3	V
17158−4049	17 19 19.6	−40 52 37	13-Sep-2008	PKS	0.09			N
17175−2819	17 20 42.5	−28 22 37	03-Mar-2010	GBT	0.020	<1.1	5	V
17233−2602	17 26 28.7	−26 04 58	06-Jun-2008	ROB	0.08	<0.7	5	V
			21-Mar-2008	GBT	0.019			
17291−2147	17 32 10.1	−21 49 59	06-Jun-2008	ROB	0.07	1.3 ± 0.7	5	V
			21-Mar-2010	GBT	0.011			
17301−2538	17 33 14.1	−25 40 24	03-Mar-2010	GBT	0.019	<1.0	5	V
17348−2906	17 38 04.2	−29 08 23	03-Mar-2010	GBT	0.022			V
17359−2902	17 39 08.0	−29 04 06	03-Mar-2010	GBT	0.020	<0.4	3, 5, 6	N
17360−2142	17 39 05.9	−21 43 52	01-Mar-2010	GBT	0.011	<0.6	5	V
17361−4159	17 39 44.3	−42 00 39	13-Sep-2008	PKS	0.13			N
17376−3448	17 40 56.3	−34 50 00	15-Sep-2008	PKS	0.07			N
17382−2531	17 41 20.1	−25 32 53	03-Mar-2010	GBT	0.019	<0.7	5	N
17385−2413	17 41 38.3	−24 14 41	01-Mar-2010	GBT	0.011	<0.6	5	M
17385−3332	17 41 52.2	−33 33 40	15-Sep-2008	PKS	0.07	<0.4	3	V
17393−2727	17 42 32.2	−27 28 28	03-Mar-2010	GBT	0.020	<0.4	3, 5, 6	N, O
17404−2713	17 43 37.2	−27 14 46	03-Mar-2010	GBT	0.019	<0.4	3, 5	N
			21-Mar-2010	GBT	0.021			
17479−3032	17 51 12.5	−30 33 44	03-Mar-2010	GBT	0.021	<0.4	3	N
17482−2501	17 51 22.5	−25 01 51	03-Mar-2010	GBT	0.018	<0.4	3, 5	N
17487−1922	17 51 44.7	−19 23 42	06-Jun-2008	ROB	0.06	<0.7	5	V
			21-Mar-2010	GBT	0.017			
17499−3520	17 53 20.4	−35 21 10	15-Sep-2008	PKS	0.07			V
17506−2955	17 53 49.3	−29 55 35	03-Mar-2010	GBT	0.021	<0.4	3	N
17516−2525	17 54 43.4	−25 26 30	01-Mar-2010	GBT	0.011	<0.3	5, 7	V
17540−2753	17 57 14.1	−27 54 16	01-Mar-2010	GBT	0.012			N
17543−3102	17 57 33.6	−31 03 03	15-Sep-2008	PKS	0.09	<0.4	3	N
17548−2753	17 57 57.8	−27 53 21	03-Mar-2010	GBT	0.019	<0.4	3	N
17550−2120	17 58 04.2	−21 21 09	03-Mar-2010	GBT	0.021	<0.4	3, 5	N, O
17550−2800	17 58 10.6	−28 00 26	03-Mar-2010	GBT	0.017	<0.8	5	V
17552−2030	17 58 16.3	−20 30 22	01-Mar-2010	GBT	0.011			N
17560−2027	17 59 04.5	−20 27 24	01-Mar-2010	GBT	0.010	<0.4	3, 5	V
17596−3952	18 03 06.7	−39 51 53	13-Sep-2008	PKS	0.11			V
18011−1847	18 04 02.7	−18 47 10	06-Jun-2008	ROB	0.07	<0.8	5	N, O
			21-Mar-2010	GBT	0.018			
18015−1352	18 04 22.2	−13 51 49	06-Jun-2008	ROB	0.06	<0.5	5	N, O
			21-Mar-2010	GBT	0.024			
18016−2743	18 04 45.8	−27 43 11	01-Mar-2010	GBT	0.012			N, O
18039−1903	18 06 53.3	−19 03 09	01-Mar-2010	GBT	0.014	11.3 ± 1.2	5	N, O
18049−2118	18 07 54.8	−21 18 09	01-Mar-2010	GBT	0.010	<4	5	N, O
18051−2415	18 08 12.8	−24 14 36	03-Mar-2010	GBT	0.018	<0.4	3	M
18071−1727	18 10 05.9	−17 26 35	01-Mar-2010	GBT	0.013	<6	6	N, O
18083−2155	18 11 18.9	−21 55 05	01-Mar-2010	GBT	0.015	<1.4	5	M
18087−1440	18 11 34.6	−14 39 56	03-Mar-2010	GBT	0.014	<0.21	3, 5, 6	N
18105−1935	18 13 32.2	−19 35 03	01-Mar-2010	GBT	0.014	<0.9	5	N
18113−2503	18 14 26.3	−25 02 56	03-Mar-2010	GBT	0.013	105.814 ± 0.003	5, 8	M
			21-Mar-2010	GBT	0.018			
18135−1456	18 16 26.1	−14 55 13	01-Mar-2010	GBT	0.014	5.3 ± 0.4	3, 5, 9, 10	N, O
18183−2538	18 21 24.7	−25 36 35	01-Mar-2010	GBT	0.012	<1.2	5	V
18199−1442	18 22 50.8	−14 40 49	01-Mar-2010	GBT	0.013	<0.8	5	N, O
18229−1127	18 25 45.0	−11 25 56	06-Jun-2008	ROB	0.06	<2.4	5	V
			21-Mar-2010	GBT	0.015			
18236−0447	18 26 20.3	−04 45 42	01-Mar-2010	GBT	0.013	<0.12	5, 10	N, O
18355−0712	18 38 15.4	−07 09 52	01-Mar-2010	GBT	0.012	<0.4	3, 5, 6	N

Table 1. continued.

IRAS name	RA (J2000)	Dec (J2000)	Observation date	Telescope[a]	rms[b] (Jy)	Previous[c] (Jy)	References[d]	Image[e]
18361−1203	18 38 58.8	−12 00 44	01-Mar-2010	GBT	0.012	<1.3	5	V
			21-Mar-2010	GBT	0.016			
18385+1350	18 40 52.1	+13 52 54	07-Mar-2010	GBT	0.015	<0.9	5	N
18434−0042	18 46 04.4	−00 38 55	01-Mar-2010	GBT	0.011	<0.9[f]	5	N
18454+0001	18 48 01.5	+00 04 48	01-Mar-2010	GBT	0.012	<1.2	5	V
18470+0015	18 49 39.1	+00 18 52	01-Mar-2010	GBT	0.013	<1.5	5	N
18485+0642	18 50 58.9	+06 45 55	06-Jun-2008	ROB	0.05	<0.4	3, 5	V
18514+0019	18 53 58.0	+00 23 25	01-Mar-2010	GBT	0.012	<1.3	5	N
18529+0210	18 55 26.3	+02 14 49	03-Mar-2010	GBT	0.018			M, O
			07-Mar-2010	GBT	0.014			
18580+0818	19 00 25.2	+08 22 47	07-Mar-2010	GBT	0.013	<0.8	5	N, O
18596+0315	19 02 06.4	+03 20 15	07-Mar-2010	GBT	0.014	18 ± 6	3, 9, 11, 12, 13	N, O
19006+1022	19 02 59.9	+10 26 35	20-Jun-2008	ROB	0.06	<0.7	5	N
			21-Mar-2010	GBT	0.013			
19011+1049	19 03 30.7	+10 53 53	07-Mar-2010	GBT	0.013			M
19013+0629	19 03 44.4	+06 34 12	20-Jun-2008	ROB	0.06	<0.8	5	N, O
19015+1256	19 03 52.6	+13 01 21	07-Mar-2010	GBT	0.013	<1.0	5	N
19071+0857	19 09 29.7	+09 02 23	09-Oct-2010[g]	VLA	0.0007	2.1 ± 0.5	5	N
19075+0432	19 10 00.0	+04 37 06	07-Mar-2010	GBT	0.013	<0.8	5, 14	V
19079−0315	19 10 32.5	−03 10 16	20-Jun-2008	ROB	0.10	<0.8	5	V
			21-Mar-2010	GBT	0.013			
19094+1627	19 11 44.6	+16 32 54	07-Mar-2010	GBT	0.013	<1.4	5	V
19134+2131	19 15 35.4	+21 36 33	07-Mar-2010	GBT	0.013	6.0 ± 2.4	15, 16, 17, 18, 19	N
19176+1251	19 19 55.9	+12 57 35	20-Jun-2008	ROB	0.08	<0.6	5	N
19178+1206	19 20 14.1	+12 12 22	07-Mar-2010	GBT	0.012	<0.4	20	N, O
19190+1102	19 21 25.3	+11 08 40	07-Mar-2010	GBT	0.013	96. ± 0.4	11, 21, 22	N
19319+2214	19 34 03.4	+22 21 14	28-Jun-2008	ROB	0.06	3.7 ± 0.5	20	N
			07-Mar-2010	GBT	0.013			
19374+2359	19 39 35.4	+24 06 25	07-Mar-2010	GBT	0.013	38 ± 15	5, 23[h]	V
20035+3242	20 05 29.6	+32 51 35	24-Sep-2008	ROB	0.08	<1.9	5	N
			07-Mar-2010	GBT	0.010			
20042+3259	20 06 10.6	+33 07 51	28-Jun-2008	ROB	0.08	<2.5	5	N
			07-Mar-2010	GBT	0.012			
20214+3749	20 23 19.2	+37 58 52	29-Jul-2008	ROB	0.06	<0.6	5	N
			07-Mar-2010	GBT	0.011			
20244+3509	20 26 25.4	+35 19 14	24-Sep-2008	ROB	0.12	<0.7	5	V
			21-Mar-2010	GBT	0.013			
20461+3853	20 48 04.6	+39 05 01	29-Jul-2008	ROB	0.06	<1.7	5	V
			21-Mar-2010	GBT	0.013			
21525+5643	21 54 15.0	+56 57 23	29-Jul-2008	ROB	0.05	<1.6	5	N
			21-Mar-2010	GBT	0.014			
21554+6204	21 56 58.3	+62 18 43	29-Jul-2008	ROB	0.05	<0.11	5, 10, 24	N, O
			21-Mar-2010	GBT	0.014			

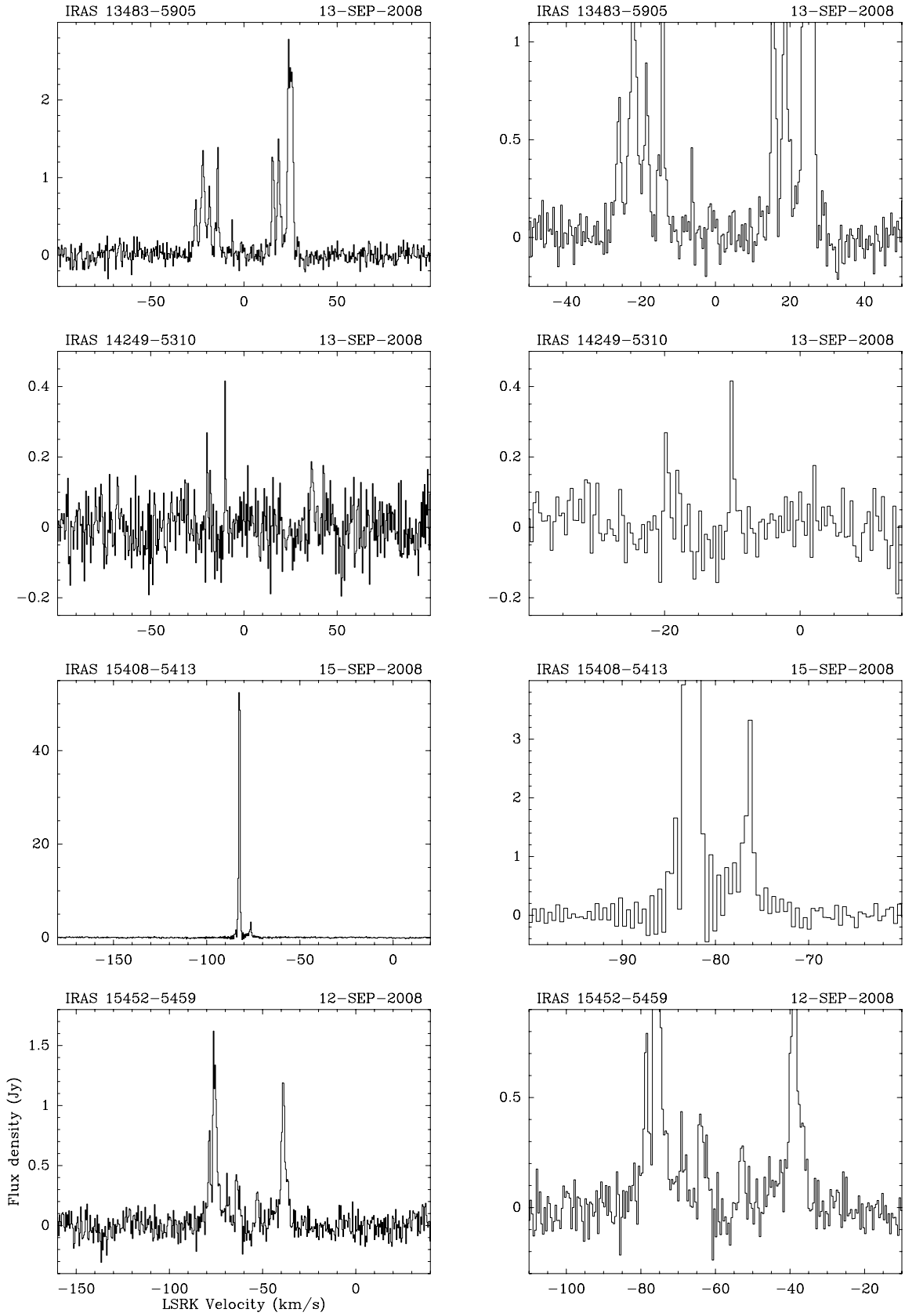

Fig. 1. Water maser spectra of the detected sources. Note that some objects were observed more than once. The *x*-axis is the velocity with respect to the local standard of rest (kinematical definition) in km s^{-1}, and the *y*-axis is flux density in Jansky. The spectra in the *left column* show the full scale in flux density, and a range of 200 km s^{-1} in velocity (except in the case of IRAS 18113−2503, which is shown with a velocity range of 600 km s^{-1}). The spectra in the *right column* are the same as the corresponding ones in the *left column*, but with a restricted scale in flux density and/or velocity, to better show weak or narrow spectral features.

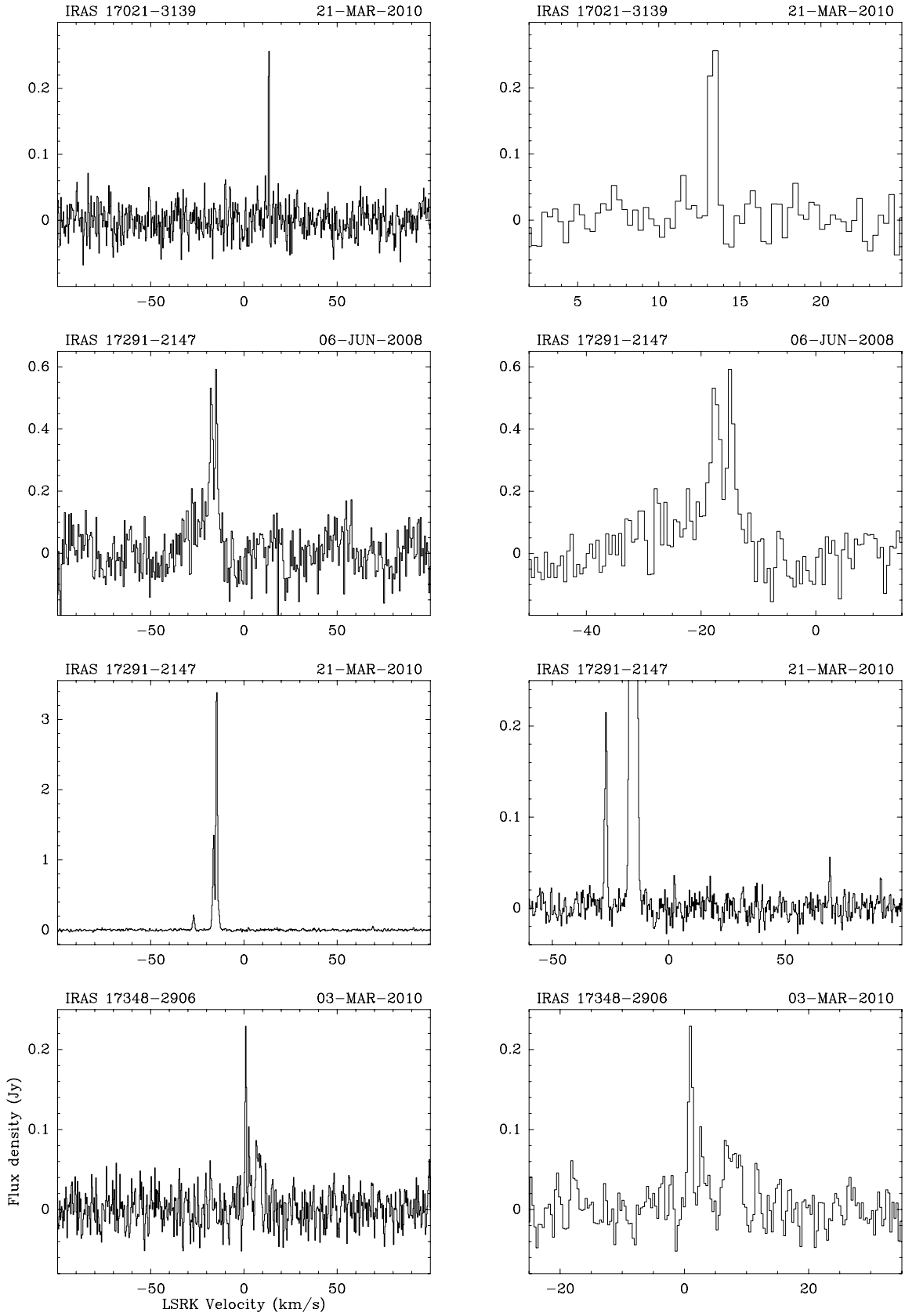

Fig. 1. continued.

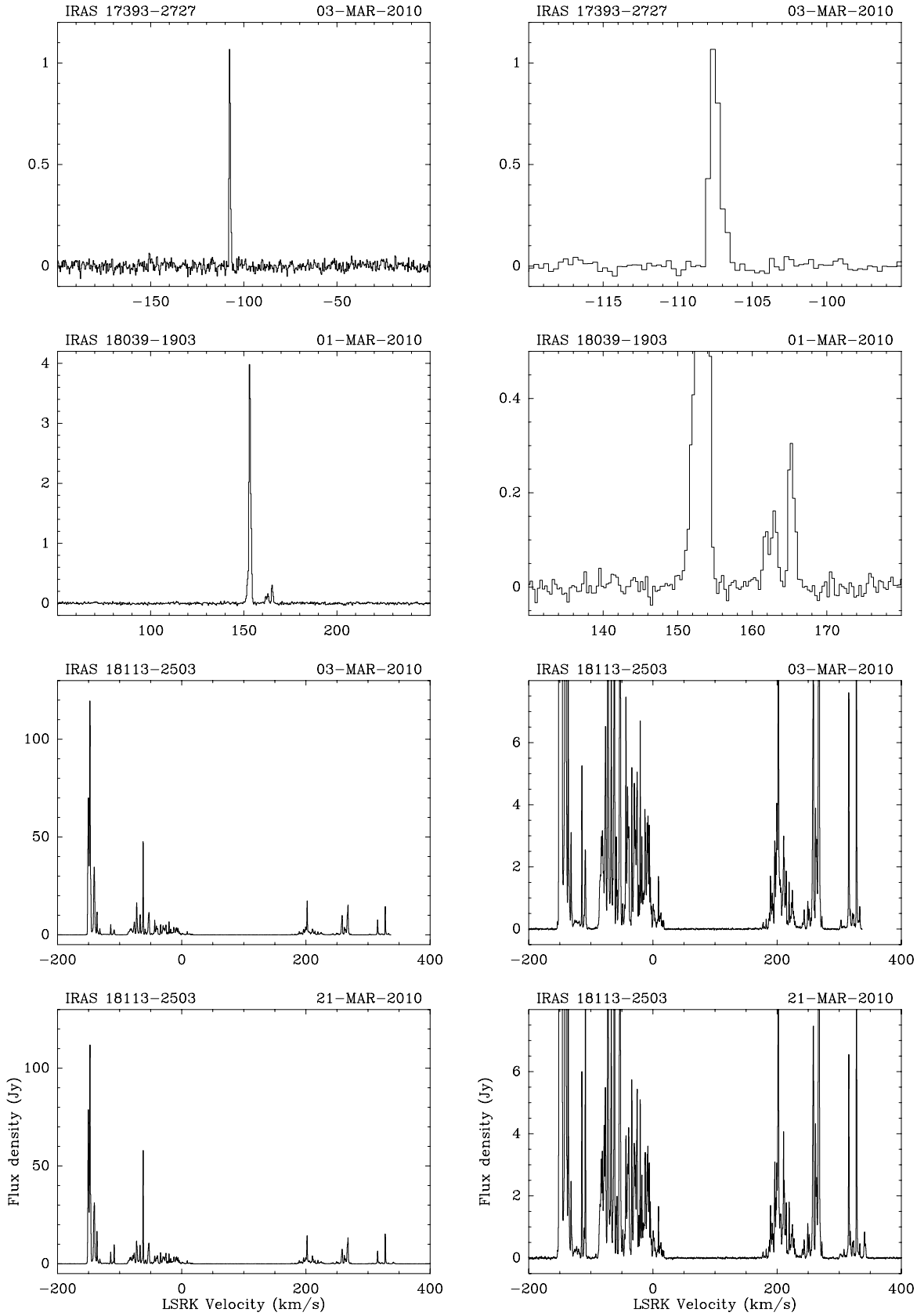

Fig. 1. continued.

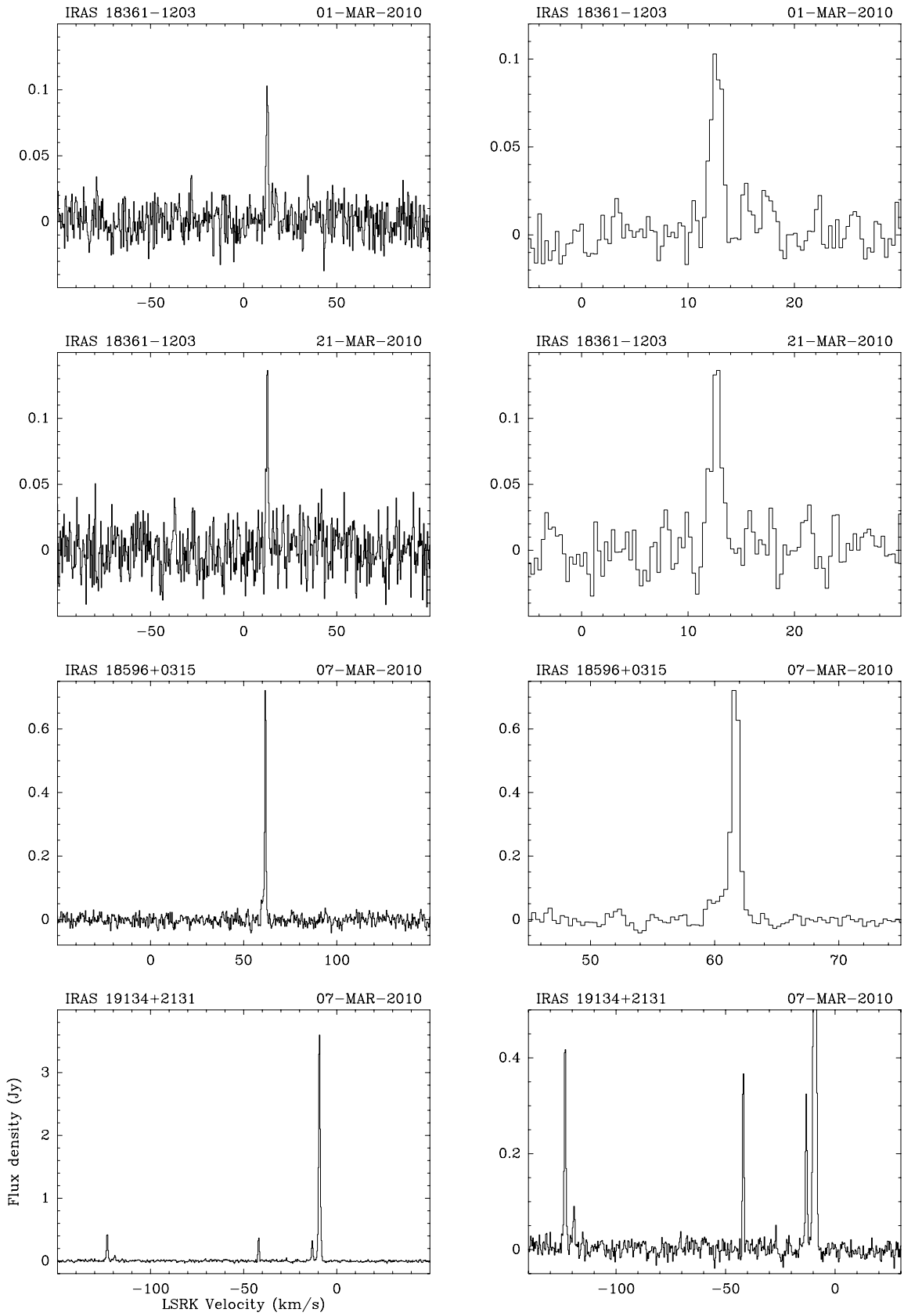

Fig. 1. continued.

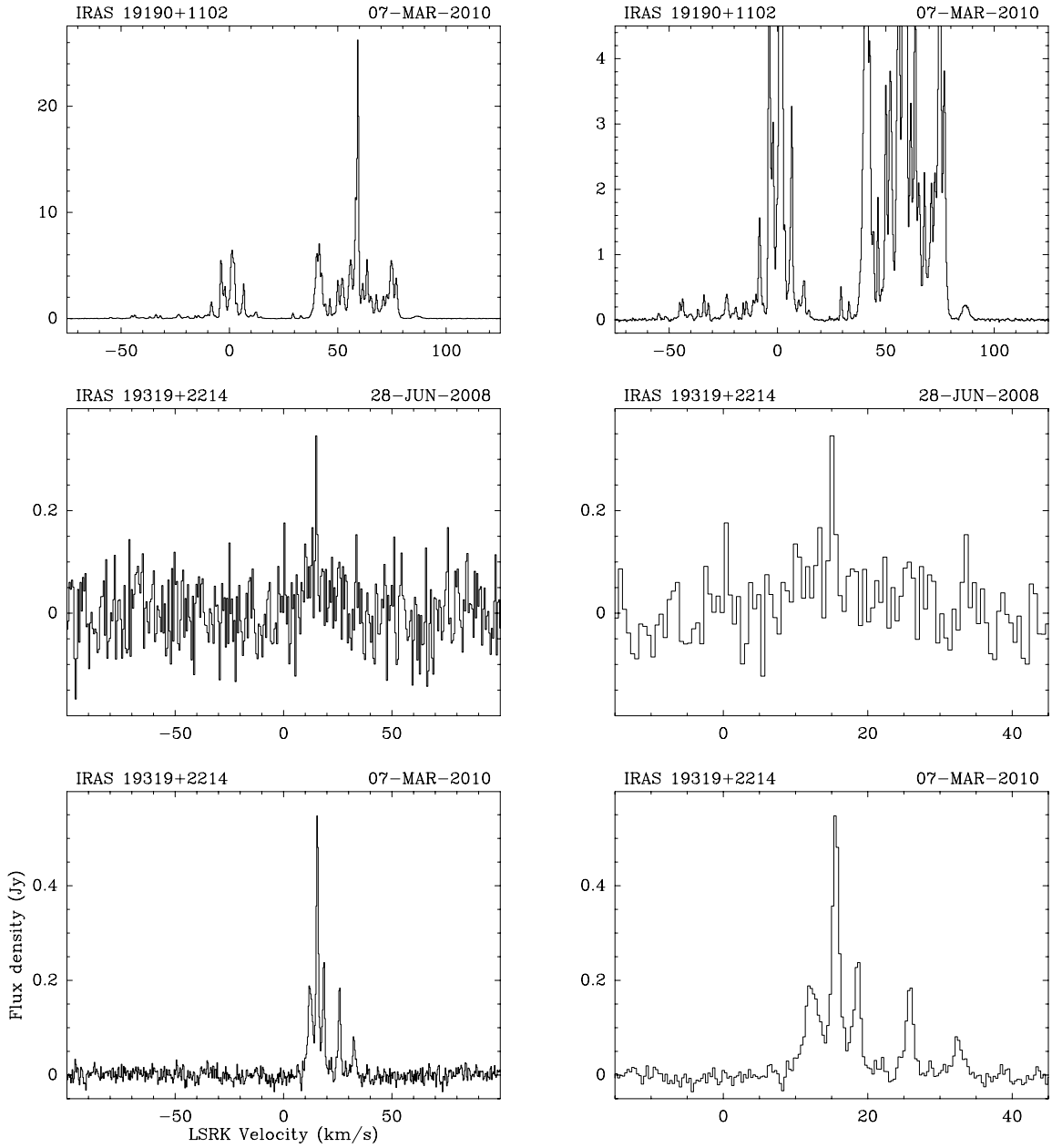

Fig. 1. continued.